THE JOURNAL OF BIOLOGICAL CHEMISTRY VOL. 292, NO. 3, pp. 898–911, January 20, 2017

Molecular Determinants of the Sensitivity to $G_{q/11}$-Phospholipase C-dependent Gating, Gd^{3+} Potentiation, and Ca^{2+} Permeability in the Transient Receptor Potential Canonical Type 5 (TRPC5) Channel*

Received for publication, August 25, 2016, and in revised form, November 24, 2016 Published, JBC Papers in Press, December 5, 2016, DOI 10.1074/jbc.M116.755470

Xingjuan Chen, Wennan Li, Ashley M. Riley, Mario Soliman, Saikat Chakraborty, Christopher W. Stamatkin, and Alexander G. Obukhov[1]

From the Department of Cellular and Integrative Physiology, Indiana University School of Medicine, Indianapolis, Indiana 46202

Edited by Roger J. Colbran

Transient receptor potential canonical type 5 (TRPC5) is a Ca^{2+}-permeable cation channel that is highly expressed in the brain and is implicated in motor coordination, innate fear behavior, and seizure genesis. The channel is activated by a signal downstream of the G-protein-coupled receptor (GPCR)-$G_{q/11}$-phospholipase C (PLC) pathway. In this study we aimed to identify the molecular mechanisms involved in regulating TRPC5 activity. We report that Arg-593, a residue located in the E4 loop near the TRPC5 extracellular Gd^{3+} binding site, is critical for conferring the sensitivity to GPCR-$G_{q/11}$-PLC-dependent gating on TRPC5. Indeed, guanosine 5′-*O*-(thiotriphosphate) and GPCR agonists only weakly activate the $TRPC5_{R593A}$ mutant, whereas the addition of Gd^{3+} rescues the mutant's sensitivity to GPCR-$G_{q/11}$-PLC-dependent gating. Computer modeling suggests that Arg-593 may cross-bridge the E3 and E4 loops, forming the "molecular fulcrum." While validating the model using site-directed mutagenesis, we found that the Tyr-542 residue is critical for establishing a functional Gd^{3+} binding site, the Tyr-541 residue participates in fine-tuning Gd^{3+}-sensitivity, and that the Asn-584 residue determines Ca^{2+} permeability of the TRPC5 channel. This is the first report providing molecular insights into the molecular mechanisms regulating the sensitivity to GPCR-$G_{q/11}$-PLC-dependent gating of a receptor-operated channel.

Transient receptor potential canonical type 5 (TRPC5)[2] channels are predominantly expressed in the nervous system. The highest levels of TRPC5 expression are found in mammalian brain regions such as the amygdala, hippocampus, cerebellum, cerebral cortex, and substantia nigra (1, 2). TRPC5 activation is implicated in regulating neurite outgrowth, growth cone morphology, and dendritic morphogenesis (3–5). In humans, TRPC5 gene mutations are associated with male mental retardation (2). TRPC5 knock-out mice exhibit deficits in motor coordination and innate fear behavior (6, 7). Genetic ablation of TRPC5 also reduces pilocarpine-induced seizures, long term potentiation, and seizure-induced neuronal cell death in the mouse hippocampus (8, 9). Plasma membrane insertion of TRPC5 in pyramidal hippocampal neurons is associated with the generation of prolonged cholinergic depolarization and bursting during epileptiform seizure discharges, suggesting that elevated TRPC5 activity may lead to an imbalance in hippocampal neuronal networks (10).

Although TRPC5 channels have critical physiological roles, the molecular mechanisms involved in regulating TRPC5 activity remain not fully elucidated. TRPC5 proteins are localized to the plasma membrane and function as Na^+- and Ca^{2+}-permeable channels. A TRPC5 channel consists of four subunits, each subunit containing six α-helical transmembrane domains (*S1–S6*, Fig. 1*A*) and a pore loop located between the S5 and S6 transmembrane domains (1, 11). The conduction pathway of the channel is formed by the S6 transmembrane domain and pore loop residues. Activation of the G-protein-coupled receptor (GPCR)-$G_{q/11}$ followed by the phospholipase C (PLC)-dependent hydrolysis of phosphatidylinositol 4,5-bisphosphate is crucial for TRPC5 opening (1, 12–14). However, the products of PLC, inositol 1,4,5-triphosphate and diacylglycerol, do not activate the TRPC5 channel when used alone or in combination (11, 12, 15).

Divalent and trivalent cations, such as Ca^{2+}, Pb^{2+}, La^{3+}, and Gd^{3+}, markedly enhance TRPC5 activity (12, 16, 17) via an extracellular cation binding site (eCBS) that consists of the two acidic glutamate residues, Glu-543 and Glu-595, located in the vicinity of the channel's extracellular pore entrance (16, 18). Glutamates Glu-543 and Glu-595 of the eCBS motif are located on two different, but adjacent, extracellular loops of TRPC5 known as E3 and E4, respectively (Fig. 1*A*). Mutation of either of these glutamates to glutamine renders TRPC5 lanthanide-insensitive (16). The double $TRPC5_{E543Q/E595Q}$ mutant lacking both Glu-543 and Glu-595 of eCBS is also lanthanide-insensitive and can be easily activated by $G_{q/11}$-PLC (18).

* This work was supported, in whole or in part, by National Institutes of Health Grants R01HL083381 and R01HL115140 (NHLBI; to A. G. O.). The authors declare that they have no conflicts of interest with the contents of this article. The content is solely the responsibility of the authors and does not necessarily represent the official views of the National Institutes of Health.

[1] To whom correspondence should be addressed: Dept. of Cellular and Integrative Physiology, Indiana University School of Medicine, 635 Barnhill Dr., MS360A, Indianapolis, IN 46202. Tel.: 317-274-8078; Fax: 317-274-3318; E-mail: aobukhov@iu.edu.

[2] The abbreviations used are: TRPC5, transient receptor potential canonical type 5; PLC, phospholipase C; GPCR, G-protein-coupled receptor; NMDG, *N*-methyl-D-glucamine; GTPγS, guanosine 5′-*O*-(thiotriphosphate); eCBS, extracellular cation binding site; ANOVA, analysis of variance; pF, picofarad.

We reasoned that a trivalent cation, such as Gd^{3+}, which coordinates to the carboxylate moieties of Glu-543 and Glu-595, may act as a bridge to stabilize these two adjacent E3 and E4 loops in a distinct conformation that enhances channel activity. This is expected to have a significant effect on the pore architecture considering that the E4 loop extends into the pore loop, which has been proposed to contain the upper gate in the TRP channels (19). Because the double $TRPC5_{E543Q/E595Q}$ mutant lacking both Glu-543 and Glu-595 of eCBS retains fully functionality (18), we reasoned that there may be some alternative mechanism for the cross-bridging of E3 and E4 loops in TRPC5. Analysis of the sequence of the E3 and E4 loops revealed the presence of arginine residues (Arg-545 and Arg-593) located two amino acids upstream and downstream of Glu-543 and Glu-595, respectively. Arginine residues are well known to be involved in salt-bridge interactions with glutamates and hydrogen bonding with main-chain carbonyl oxygens in proteins (20, 21). We hypothesized that these arginine residues may cross-bridge the E3 and E4 loops in TRPC5 to regulate its activation downstream of the GPCR-$G_{q/11}$-PLC pathway.

Results

$TRPC5_{R593A}$ Exhibits a Reduced Sensitivity to $G_{q/11}$-PLC Activation—Wild type TRPC5 is activated by GTPγS and substantially enhanced by Gd^{3+} (Fig. 1*B*). To determine whether the Arg-545 residue located near Glu-543 on the E3 loop of TRPC5 played a role in regulating TRPC5 activity, we mutated it to alanine. We expressed this mutant in HEK cells and used dialysis of GTPγS (500 μM) to activate it via the $G_{q/11}$-protein-dependent mechanism (22). Large GTPγS-induced inward currents were observed in HEK-$TRPC5_{R545A}$ cells ($I = -96.6 \pm 27.5$ pA/pF; Fig. 1, *C* and *E*). The kinetics of current onset and decay were variable in different recordings but similar to those observed in HEK-TRPC5 cells. Both TRPC5 and $TRPC5_{R545A}$ currents presented with similar current-voltage relationships. Gd^{3+} increased the $TRPC5_{R545A}$ currents (Fig. 1, *C* and *J*) to the same extent as it potentiated the wild type TRPC5 currents (2-fold increase; Fig. 1, *B* and *J*). Thus, it appears that Arg-545 is unlikely to be involved in TRPC5 activity regulation.

We then mutated Arg-593 to alanine in TRPC5 and assessed the functional activity of the mutated channel. Strikingly, the mean density of GTPγS-induced currents in HEK-$TRPC5_{R593A}$ cells was 45-fold smaller ($I = -2.09 \pm 0.64$ pA/pF) than that in HEK-TRPC5 cells ($I = -94.9 \pm 19.7$ pA/pF; Fig. 1, *D* and *E*) at the holding potential of −100 mV. To rule out the possibility of reduced surface expression of the mutant, we compared the current densities of strong depolarizing pulse-activated (to +150 mV) (23) TRPC5, $TRPC5_{R545A}$, and $TRPC5_{R593A}$ currents. We found that the depolarization-activated $TRPC5_{R593A}$ currents were only 3-fold smaller than that for TRPC5 (TRPC5, $I = 35.37 \pm 6.11$ pA/pF; $TRPC5_{R545A}$, $I = 37.25 \pm 7.74$ pA/pF; $TRPC5_{R593A}$, $I = 11.44 \pm 1.17$ pA/pF; Fig. 1, *F* and *G*), suggesting that factors other than cell-surface expression may be responsible for the reduced amplitude of GTPγS-activated current densities in HEK-$TRPC5_{R593A}$ cells. To obtain additional evidence that the $TRPC5_{R593A}$ mutant is properly targeted to the plasma membrane, we next used the cell-surface protein biotinylation approach. We found the relative amounts of cell-surface-biotinylated TRPC5 and $TRPC5_{R593A}$ proteins were not significantly different (Fig. 1, *H* and *I*, *upper panel*). Normalization of the cell-surface biotinylated protein band densities of TRPC5 and $TRPC5_{R593A}$ to those of Na^+,K^+-ATPase revealed that the mean protein amount of the $TRPC5_{R593A}$ mutant in the plasma membrane was slightly greater than that of TRPC5 (one-tailed p value = 0.04; Two-tailed p value = 0.08, unpaired t test, Fig. 1*I*, *lower panel*).

Gd^{3+} Rescues $G_{q/11}$-PLC Sensitivity of $TRPC5_{R593A}$—We reasoned that the positively charged residue at the 593 position may act as a critical stabilizing bridge between the E3 and E4 loops. The substitution of the residue with alanine might prevent TRPC5's activation triggered by a signal downstream of the $G_{q/11}$-PLC pathway because there is no background bridging of the E3 and E4 in $TRPC5_{R593A}$ in the absence of a trivalent cation. Therefore, we examined whether Gd^{3+}-induced eCBS-dependent bridging of E3 and E4 loops would be capable of rescuing $G_{q/11}$-PLC-dependent activation of $TRPC5_{R593A}$. Indeed, we observed that the $TRPC5_{R593A}$ currents were robustly increased by extracellular Gd^{3+} in HEK-$TRPC5_{R593A}$ cells dialyzed with GTPγS. These currents exhibited the typical TRPC5-like current-voltage relationship (Fig. 1*D*) and a very fast onset as one would expect from a ligand-gated ion channel. Notably, the apparent Gd^{3+}-dependent potentiation of the inward currents was much greater in HEK-$TRPC5_{R593A}$ cells as compared with that observed in HEK-TRPC5 cells (HEK-TRPC5: I_b/I_a ratio = 2.39 ± 0.39 at −100 mV and 1.67 ± 0.23 at +100 mV; HEK-$TRPC5_{R593A}$: I_b/I_a ratio = 13.14 ± 1.53 at −100 mV and 1.86 ± 0.14 at +100 mV; Fig. 1, *B*, *D*, *G*, *J*, and *K*). These data support the hypothesis that Arg-593 may be a bridging residue between the E3 and E4 loops of TRPC5.

Histamine-induced $TRPC5_{R593A}$ Currents Are Small, and Gd^{3+} Markedly Potentiates Them—We next determined whether a stronger G-protein activation via GPCR stimulation would be a more efficient way for inducing the $TRPC5_{R593A}$ currents. We used histamine to stimulate TRPC5 via the H1 histamine receptor activation in HEK cells as described previously (23–26). Indeed, histamine led to a nearly 2-fold larger inward current in HEK-$TRPC5_{R593A}$ cells ($I_i = -3.38 \pm 0.50$ pA/pF at −100 mV; Fig. 2, *C* and *E*) compared with that observed during our GTPγS dialysis experiments (Fig. 1*D*). However, these currents were still 41-fold smaller than the inward currents activated by histamine in HEK-TRPC5 cells, H1 receptor expressing cells ($I_b = -139.19 \pm 27.36$ pA/pF at −100 mV; Fig. 2, *A* and *E*). The histamine-induced $TRPC5_{R593A}$ currents were greatly increased in the presence of extracellular Gd^{3+} ($I_j/I_{j'} = 14.27 \pm 3.38$ at −100 mV and 1.66 ± 0.27 at +100 mV, compared with $I_c/I_{c'} = 2.35 \pm 0.23$ at −100 mV and 1.27 ± 0.15 at +100 mV for TRPC5; Fig. 2, *A*, *C*, *F*, and *G*), suggesting that $TRPC5_{R593A}$ was in a histamine-insensitive state in the absence of Gd^{3+}. The Gd^{3+}-potentiated currents exhibited a fast onset and could be readily reversed to the initial current level by washing with the standard extracellular solution (Fig. 2*C*). These data indicate that even a stronger stimulus was not sufficient to overcome the apparent deficiency of $TRPC5_{R593A}$.

Extracellular Ca^{2+} Inhibits Small Histamine-induced $TRPC5_{R593A}$ Current in the Absence of Gd^{3+}—The mean current density for the wild type TRPC5 currents was 8-fold

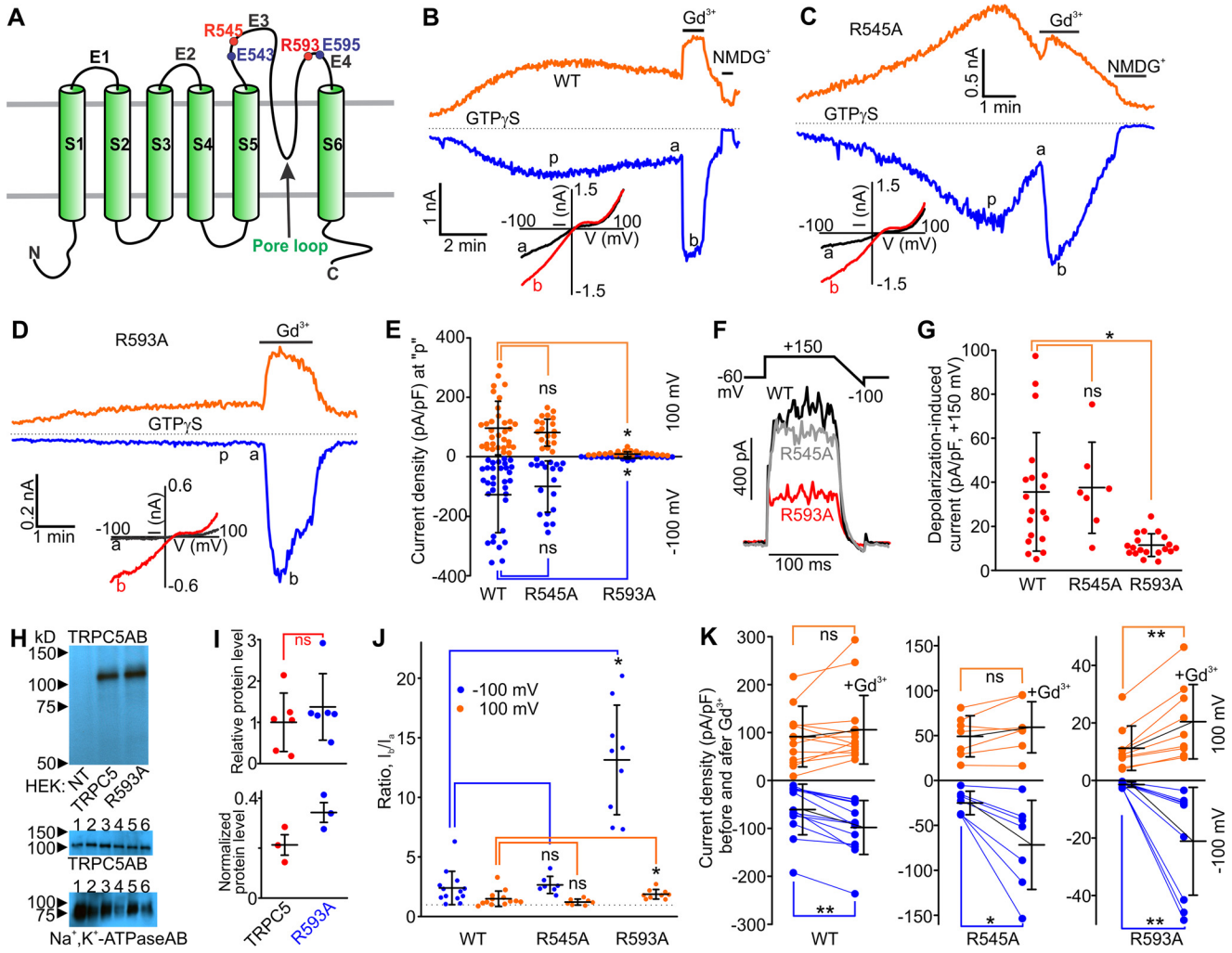

FIGURE 1. **The putative membrane topology of mouse TRPC5 and effects of Gd^{3+} on GTPγS-activated currents in mouse $TRPC5_{R545A}$- and mouse $TRPC5_{R593A}$-expressing HEK cells.** *A*, the TRPC5 subunit contains six transmembrane helices (S1-S6). The eCBS consists of the two acidic residues Glu-543 and Glu-595 (*solid blue circles*) located on E3 and E4 loops. The arginine residues Arg-545 and Arg-593 are shown with the *solid red circles*. *B–D*, sample traces of TRPC5 currents induced by a dialysis of GTPγS via the patch pipette. Gd^{3+} (100 μM) or NMDGCl was added at the times indicated by the *horizontal bars*. The *broken lines* indicate the level of the zero current. The *upper* and *lower traces* represent the outward and inward whole cell currents recorded at +100 mV (*orange lines*) and −100 mV (*blue line*). *Insets* show the current-voltage relations acquired during the voltage ramps from −100 mV to +100 mV in the absence (*black lines*) and presence (*red lines*) of Gd^{3+} at the time points indicated with *a* and *b* in the same experiment. *E*, comparison of the mean current densities of GTPγS-activated currents measured at *p* in (*B–D*). *F*, sample traces of TRPC5, $TRPC5_{R545A}$, and $TRPC5_{R593A}$ currents activated by the depolarizing pulses to +150 mV from a holding potential of −60 mV. *G*, comparison of the densities of TRPC5, $TRPC5_{R545A}$, and $TRPC5_{R593A}$ currents activated by the depolarizing pulses to +150 mV. The current density values were averaged within a 20-ms interval. *H*, Western blot analysis of cell-surface biotinylated proteins isolated from HEK cells overexpressing nothing, TRPC5, or $TRPC5_{R593A}$. The *upper Western blot* confirms the specificity of the TRPC5 antibody (*NT* = non-transfected HEK lysate). The *middle* and *lower images* show the results of Western blot analyses of cell-surface biotinylated proteins probed with the TRPC5 antibody or the Na^+,K^+-ATPase antibody, respectively (six independent biotinylation experiments). The exposure times were 10 s for the TRPC5 antibody and 30 s for the Na^+,K^+-ATPase antibody. *1*, *2*, and *3* indicate the lanes where biotinylated proteins from HEK-TRPC5 cells were separated, whereas *4*, *5*, and *6* indicate the lanes where biotinylated proteins from HEK-$TRPC5_{R593A}$ cells were separated. *I*, densitometry analyses of the data shown in *H*. The *upper panel* shows a comparison of amounts of cell-surface biotinylated $TRPC5_{R593A}$ proteins relative to that of cell-surface biotinylated TRPC5 proteins. The *lower panel* shows a comparison of biotinylated protein band densities of TRPC5 and $TRPC5_{R593A}$ normalized to that of Na^+,K^+-ATPase. *J* and *K*, summary data of current ratios and densities measured at the time points of *a* and b″, before and after Gd^{3+} addition to the bath, at the holding potentials of −100 mV (*blue dots*), and +100 mV (*orange dots*) for the data sets shown in *B–D*. In all three plots of *K*, the *y* axis label is *Current densities before and after Gd^{3+} application*. The ratios quantify the relative current amplitude increases in the presence of Gd^{3+}. One-way ANOVA on Rank followed by the all-pairwise comparison Dunn's test was used in *E*, *G*, and *J*, the unpaired *t* test was used in *I*, and the before and after treatment Wilcoxon Signed Rank Test was used in *K* to determine whether there is a significant difference between the tested groups (*, $p < 0.05$; **, $p < 0.01$). *ns* stands for not significant. The *vertical error bars* represent standard deviations, and the mean values are indicated with *horizontal bars*.

smaller (I_e = −18.19 ± 3.81 pA/pF at −100 mV; Fig. 2, *B*, *E*, and *H*) in the absence of extracellular Ca^{2+}, and the current density significantly increased in the presence of 2 mM extracellular Ca^{2+} (I_f = −48.89 ± 17.87 pA/pF at −100 mV; Fig. 2, *B* and *H*), consistent with the data reported by Okada *et al.* (1). In contrast, the histamine-induced $TRPC5_{R593A}$ current density (I_l = −7.62 ± 0.96 pA/pF at −100 mV; Fig. 2, *D* and *H*) was greater in the presence of Ca^{2+}-free extracellular solution, and subsequent re-addition of 2 mM Ca^{2+} significantly inhibited the outward $TRPC5_{R593A}$ current (I_l = 35.27 ± 4.76 pA/pF *versus* I_m = 19.75 ± 3.62 pA/pF at +100 mV; Fig. 2, *D* and *H*).

Pretreatment with Gd^{3+} Sensitizes $TRPC5_{R593A}$ to Histamine-dependent Activation—TRPC5 is activated by an unidentified stimulus that is downstream of the G-protein-PLC pathway. It

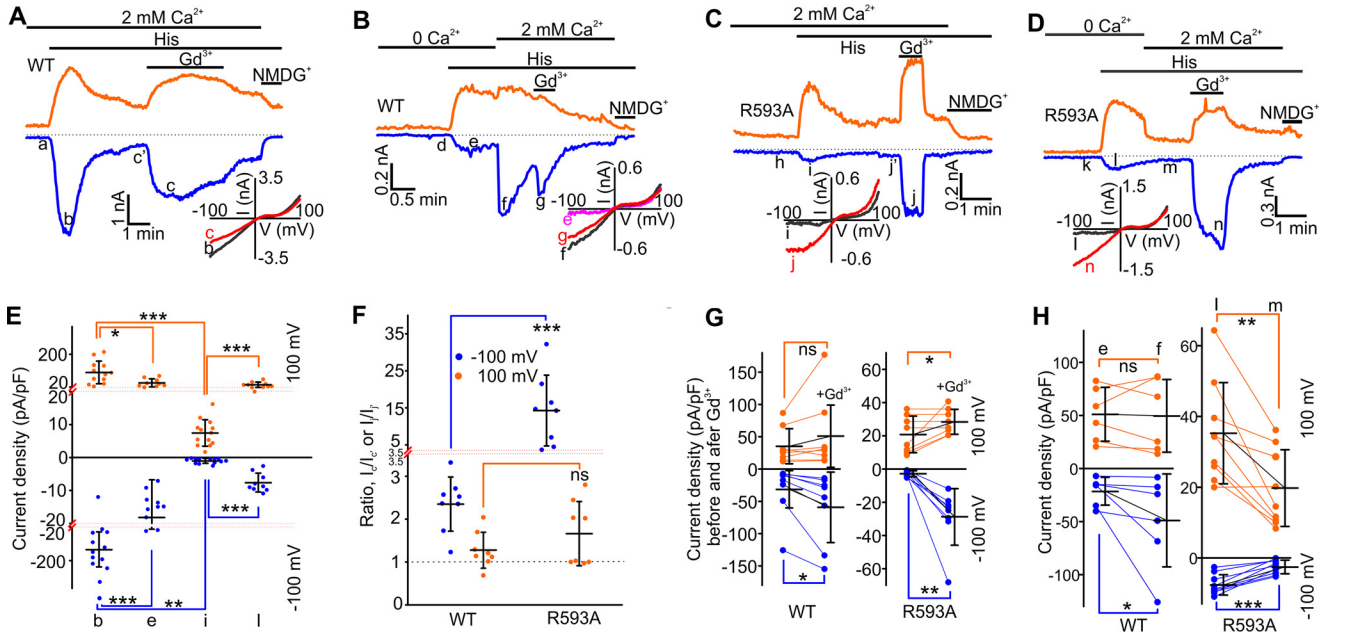

FIGURE 2. **Effects of Gd^{3+} or Ca^{2+} on histamine-induced currents in mouse TRPC5- and mouse $TRPC5_{R593A}$-expressing HEK cells.** *A–D*, sample traces of time courses for currents via TRPC5 or $TRPC5_{R593A}$. Histamine (5 μM), Gd^{3+} (100 μM), Ca^{2+} (2 mM), and NMDGCl were added at the times indicated by the *horizontal bars*. The *broken lines* indicate the level of the zero current. The *upper traces* represent the outward whole cell currents recorded at +100 mV (*orange lines*), whereas the *lower traces* represent the inward currents recorded at −100 mV (*blue lines*). *Insets* show the current-voltage relationships acquired during the voltage ramps from −100 mV to +100 mV in the absence (*black lines*) and presence (*red lines*) of Gd^{3+} in the same experiment. *E*, comparison of current densities measured at the indicated points (*b*, *e*, *i*, *l*) at the holding potentials of −100 (*blue dots*) and +100 mV (*orange dots*). *F*, comparison of the current ratios of I_c/I_c' or I_j/I_j' characterizing Gd^{3+}-induced potentiation at the holding potentials of −100 (*blue dots*) and +100 mV (*orange dots*). *G*, comparison of current densities measured before and after the addition of Gd^{3+} at the holding potentials of −100 (*blue dots*) and +100 mV (*orange dots*). *H*, comparison of current densities before and after re-addition of 2 mM Ca^{2+}. In *E* and *F*, the *red dotted lines* show the positions where the *y* axis scale changes. The Mann-Whitney Rank Sum test was used in *E* and *F*, whereas the Wilcoxon Signed Rank Test was used in *G* and *H* to determine whether there is a significant difference between the tested groups (*, $p < 0.05$, **, $p < 0.01$, ***, $p < 0.001$). *ns* stands for not significant. The *vertical error* bars represent standard deviations, and the mean values are indicated with *horizontal bars*.

is possible that the $TRPC5_{R593A}$ mutant may simply exhibit a decreased sensitivity to such a stimulus. Due to a fast decay rate of TRPC5 currents, we used histamine concentration ramps (0.01 μM - 0.1 μM - 1 μM - 10 μM - 100 μM - 300 μM; each concentration was applied for ~30 s; Fig. 3, *A–D*) to estimate apparent EC_{50} values for histamine-dependent TRPC5 and $TRPC5_{R593A}$ activation in the presence and absence of Gd^{3+}. We found that the EC_{50} values for histamine were as follows: 1.2 μM in HEK-TRPC5 cells in the absence of Gd^{3+}; 1.5 μM in HEK-TRPC5 cells in the presence of Gd^{3+}; 0.9 μM HEK-$TRPC5_{R593A}$ cells in the absence of Gd^{3+}; 1.1 μM in the presence of Gd^{3+} (Fig. 3*E*). In the absence of Gd^{3+} even 300 μM histamine activated only small $TRPC5_{R593A}$ currents as compared with those observed in HEK-TRPC5 cells (Fig. 3, *A*, *C*, and *F*). Conversely, pretreatments with Gd^{3+} potently sensitized the $TRPC5_{R593A}$ mutant to histamine activation (I_c = −3.26 ± 1.30 pA/pF compared with I_e = −121.05 ± 28.14 pA/pF; Fig. 3, *D* and *F*).

The mean amplitude of 300 μM histamine-activated TRPC5 was significantly smaller in the presence of Gd^{3+} compared with the wild type TRPC5 currents observed in the absence of Gd^{3+} (3-fold, Fig. 3, *A*, *B*, and *F*). These data suggest that Gd^{3+} not only potentiates but may also inhibit TRPC5 by blocking its pore. This is in agreement with the report by Jung *et al.* 2003 (16). We next compared the mean densities of TRPC5 and $TRPC5_{R593A}$ currents obtained in the presence of Gd^{3+}. The values of the mean current densities were not significantly different (Fig. 3*F*), indicating Gd^{3+} completely rescued the ability of $TRPC5_{R593A}$ to conduct currents when the mutant is activated by histamine. This again suggests that preassembling of the eCBS with Gd^{3+} in the absence of Arg-593 is sufficient to rescue $G_{q/11}$-PLC-dependent activation sensitivity of $TRPC5_{R593A}$, further supporting the hypothesis that Arg-593 serves as a bridging element ensuring the integrity of the eCBS.

A Model of the Three-Dimensional Structure of TRPC5—To gain insight into the molecular mechanisms underlying the effect of Arg-593 on TRPC5's $G_{q/11}$-PLC activation sensitivity, we constructed a model of the pore region of TRPC5 in the open state using the cryo-EM atomic coordinates of the TRPV1 structure as a template. The model predicts that the Glu-543 and Glu-595 residues are located close to each other at the extracellular surface of the protein (Fig. 4*A*), and the distance between Arg-593 and either Glu-543 or Glu-595 exceeded 4 Å, excluding the possibility of ionic and hydrogen bonding interactions. Subsequent short molecular dynamics simulations were used to enable the side chains of the residues from the homology model to adopt their optimal positions. The final structure reveals that Glu-543, Glu-595, and Arg-593 may adopt different conformations in TRPC5 (Fig. 4, *B–D*). In our model, Gd^{3+} coordinates with the oxyanions of Glu-543 and Glu-595 such that the ion bridges the E3 and E4 loops (Fig. 4, *E* and *F*). Interestingly, in the absence of Gd^{3+}, the E3 and E4 loops can also interact through a salt-bridge interaction between Arg-593 and Glu-543 and/or hydrogen bonding to main-chain carbonyl oxygen groups (Fig. 4*B*).

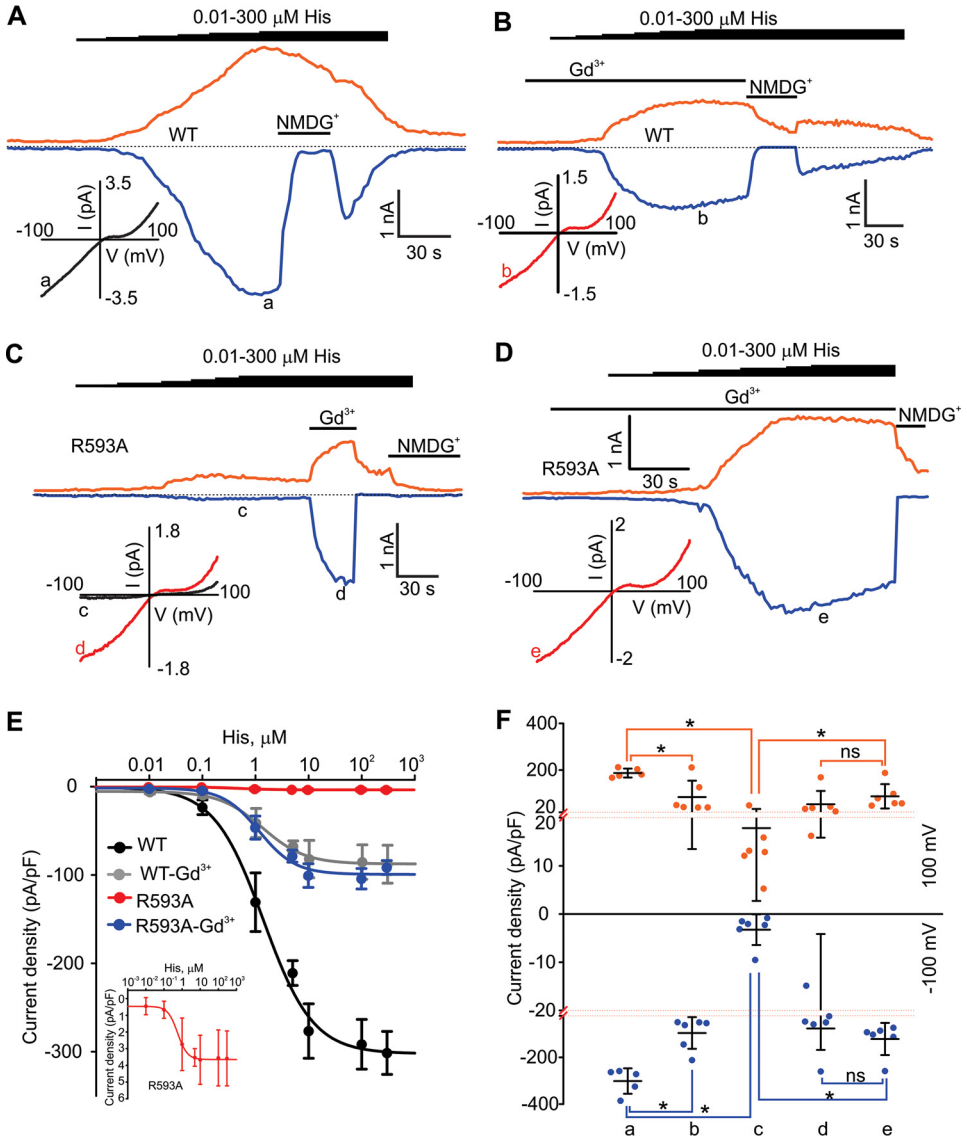

FIGURE 3. **Dose-response curves for histamine in mouse TRPC5- and mouse TRPC5$_{R593A}$-expressing HEK cells.** *A–D*, sample traces of the currents induced by incremental increases in concentration of histamine in HEK cell expressing TRPC5 or TRPC5$_{R593A}$. Histamine (0.01, 0.1, 1, 10, 100, 300 μM), Gd^{3+} (100 μM), and NMDGCl were added at the time points indicated by the *horizontal bars*. The *broken lines* indicate the level of the zero current. The *upper traces* represent the outward whole cell currents recorded at +100 mV (*orange lines*), whereas the *lower traces* represent the inward currents recorded at −100 mV (*blue lines*). *Insets* show the current-voltage relations acquired during the voltage ramps from −100 mV to +100 mV at the time points indicated with *a–e*. *E*, the dose-response curves for histamine obtained in HEK-TRPC5 cells ($n = 5$) and HEK-TRPC5$_{R593A}$ cells ($n = 6$) in the presence or absence of Gd^{3+} (100 μM). The *inset* shows the dose-response curve for histamine with an expended *y* axis scale obtained in HEK-TRPC5$_{R593A}$ cells in the absence of Gd^{3+}. *F*, comparison of current densities of histamine-activated currents recorded at −100 mV (*blue dots*) and +100 mV (*orange dots*) measured at different points in *A–D*. The *red dotted lines* show the positions where the *y* axis scale changes. The *vertical error bars* represent standard deviations, and the mean values are indicated with *horizontal bars* (*, $p <$ 0.05, Mann-Whitney Rank Sum test).

The models further reveal additional features of TRPC5's molecular organization. First, we noticed that there are several aromatic residues, Phe-540, Tyr-541, and Tyr-542 (Fig. 4*C*), located just below the Glu-543 residue at the base of the E3 loop. These hydrophobic side chains likely further stabilize the interaction between the E3 and E4 loops through the hydrophobic effect. Secondly, it appears that the polar main-chain carbonyl group of Tyr-542 may contribute to coordinating Gd^{3+} within the eCBS (Fig. 4, *E* and *F*), suggesting a role for the residue in regulating Gd^{3+} sensitivity of TRPC5. Finally, we noted that Asn-584 occupies the position that is homologous to Asp-646 of TRPV1, identified as the TRPV1's selectivity filter (Figs. 4*C* and 7*A*). This suggests that Asn-584 may be involved in modulating Ca^{2+} permeability in TRPC5. To validate the models, we next explored whether the identified residues affect either Gd^{3+} sensitivity or Ca^{2+} permeability in TRPC5.

Non-acidic Residues Modulate Gd^{3+} Sensitivity in TRPC5—To determine the role of the identified aromatic residues (Figs. 4*C* and 5*A*; *F540*, *Y541*, and *Y542*) neighboring Glu-543, we first substituted an alanine for the Tyr-541 residue. Like the wild type TRPC5, TRPC5$_{Y541A}$ can be easily activated by GTPγS dialysis and exhibited large, slowly developing inward currents with a characteristic non-linear current-voltage relationship ($I_{WT} = -64.73 \pm 17.66$ pA/pF and $I_{Y541A} = -108.93 \pm 16.01$ pA/pF at −100 mV; Fig. 5, *B* and *F*). We next tested whether the

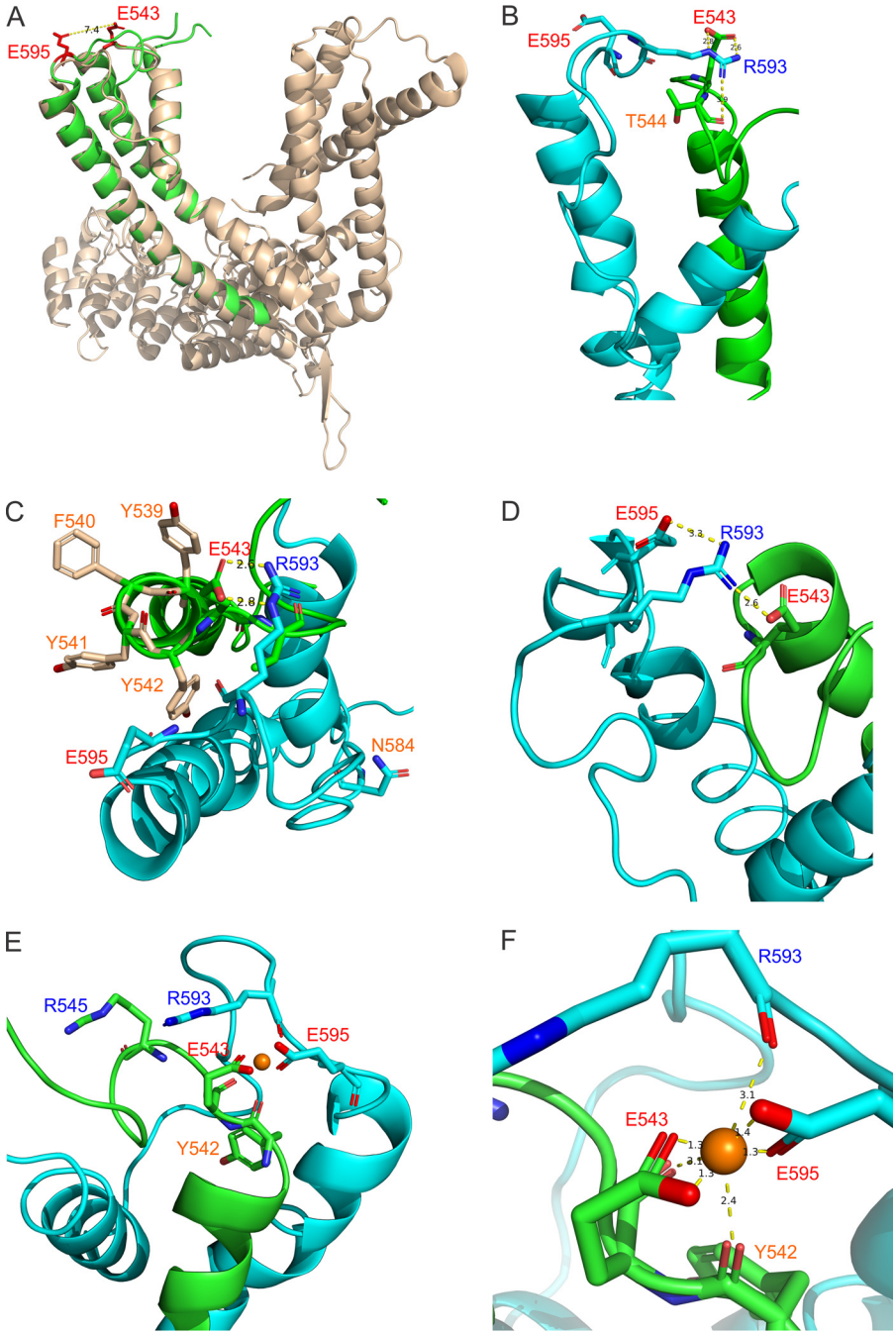

FIGURE 4. **Homology modeling and molecular dynamics simulations.** *A*, superimposed mouse TRPC5 homology model (*green*) and the cryo-EM structure of the rat TRPV1 channel (*wheat*) in the open state. Glu-543 and Glu-595 residues in TRPC5 are colored *red*. *B–D*, The interatomic interactions are depicted in the selected conformations predicted from molecular dynamics simulations. The S5 domain and the E3 loop are colored in *green*. The S6 domain, E4 loop, and the pore helix are colored in *sky blue*. Interatomic distances in angstroms are shown as *black numbers next to the yellow broken lines*. *E* and *F*, the interatomic Gd^{3+} (the *orange ball*) and side chain interactions within the eCBS predicted from molecular dynamics simulations. The color coding is as in *B–D*.

$TRPC5_{Y541A}$ currents are potentiated by extracellular Gd^{3+}, a signature property of wild type TRPC5. We unexpectedly found that Gd^{3+} did not potentiate the GTPγS-induced $TRPC5_{Y541A}$ activity (0.98 ± 0.08-fold change at −100 mV and 0.86 ± 0.07-fold change at +100 mV; Fig. 5, *B*, *G*, and *H*), suggesting that the Tyr-541 residue may be important for regulating the TRPC5's Gd^{3+} sensitivity.

Because it has been reported that $TRPC5_{E543Q}$ exhibits no Gd^{3+} sensitivity (16, 18), we compared the Gd^{3+} sensitivity of $TRPC5_{Y541A}$ with that of $TRPC5_{E543Q}$. In HEK-$TRPC5_{E543Q}$ cells, GTPγS dialysis induced the inward currents that were comparable with those observed in HEK-TRPC5 and HEK-$TRPC5_{Y541A}$ cells. We found that Gd^{3+} significantly inhibited the $TRPC5_{E543Q}$ currents (0.6-fold change at −100 mV and 0.7-fold change at +100 mV; Fig. 5, *C*, *G*, and *H*), most likely due to its ability to block the pore of cation channels (16). In contrast, Gd^{3+} did not inhibit the GTPγS-induced $TRPC5_{Y541A}$ currents. Hence, the $TRPC5_{Y541A}$ mutant may still exhibit some sensitivity to Gd^{3+} that is masked by the dominance of the pore blocking effect. Indeed, Gd^{3+} slightly (1.3-fold change

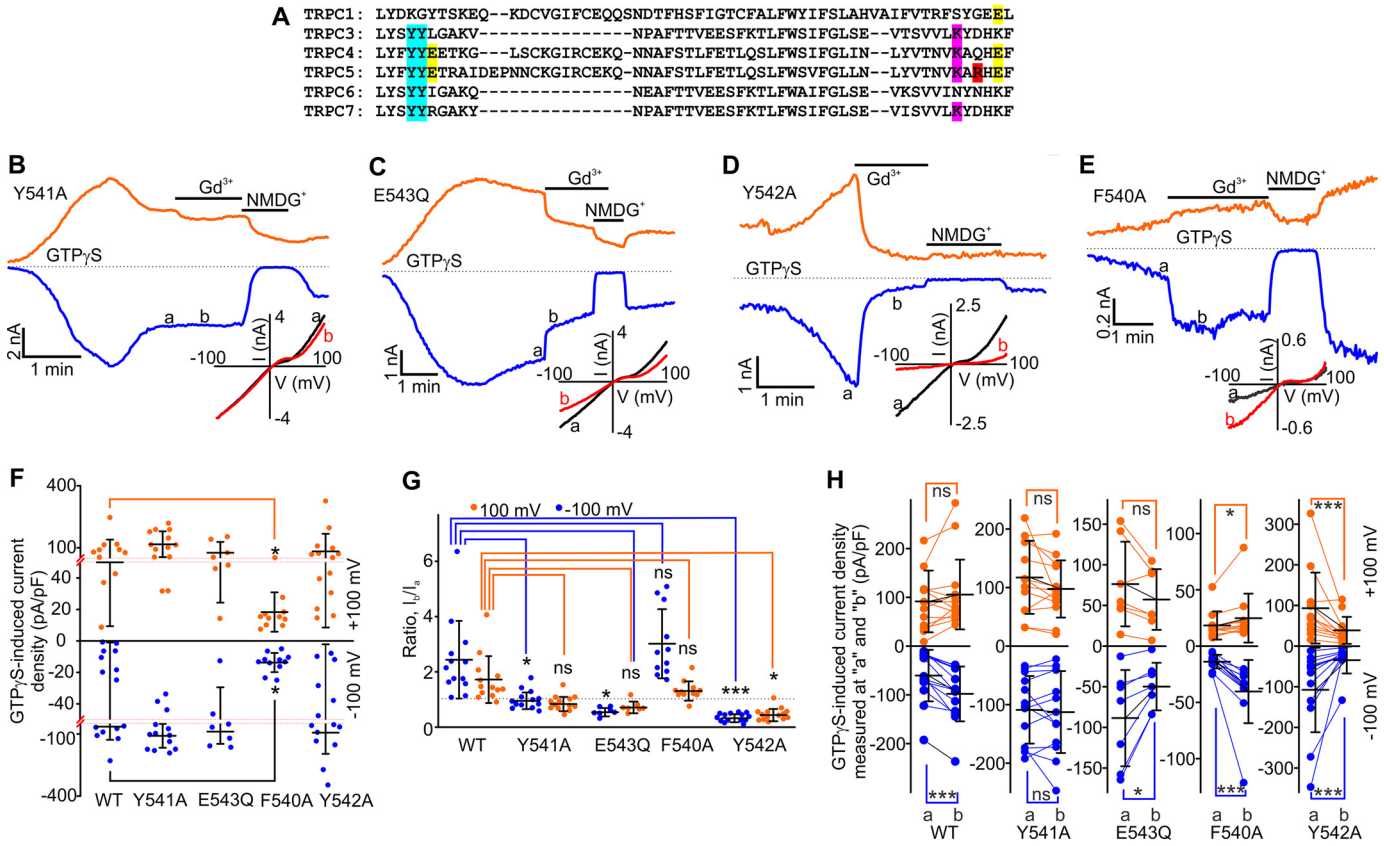

FIGURE 5. **Effects of Gd^{3+} on GTPγS-activated currents mediated by mouse TRPC5, mouse $TRPC5_{Y541A}$, mouse $TRPC5_{E543Q}$, mouse $TRPC5_{Y542A}$, and mouse $TRPC5_{F540A}$.** *A*, the sequence alignment for mouse TRPC1, TRPC3, TRPC4, TRPC5, TRPC6, and TRPC7. The TRPC5's Tyr-541 and Tyr-542 residues are highlighted in *sky blue*. The glutamate residues Glu-543 and Glu-595 are highlighted in *yellow*. The Arg-593 residue in TRPC5 is highlighted in *red*. *B–E*, time courses of the whole-cell currents induced by a dialysis of 500 μM GTPγS in HEK cells overexpressing TRPC5 or one of the mutants listed above. Gd^{3+} (100 μM) and NMDGCl were added at the times indicated by the *horizontal bars*. The *broken lines* indicate the level of the zero current. The *upper* and *lower traces* represent the outward and inward whole cell currents recorded at +100 mV (*orange lines*) and −100 mV (*blue lines*). *Insets* show the current-voltage relations recorded in the absence (*black lines*) and presence (*red lines*) of Gd^{3+}. *F*, comparison of the mean current densities of GTPγS-activated currents recorded at −100 mV (*blue dots*) and +100 mV (*orange dots*) in HEK cells transfected with TRPC5-WT, $TRPC5_{Y541A}$, $TRPC5_{Y542A}$, $TRPC5_{F540A}$, or $TRPC5_{E543Q}$. The *red dotted lines* show the positions where the *y* axis scale changes. *G* and *H*, summary data of current ratios and current densities measured at the time points of *a* and *b* at holding potentials of −100 mV (*blue dots*) and +100 mV (*orange dots*) for the data sets shown in *B–E*. The ratios quantify the relative current amplitude increases in the presence of Gd^{3+}. In all five plots of *H*, the *y* axis label is *GTPγS-induced current density measured at a and b (pA/pF)*. The *vertical error bars* represent standard deviation, and the mean values are indicated with *horizontal bars* (*, $p < 0.05$; ***, $p < 0.001$; *ns*, stands for not significant; one-way ANOVA on Rank followed by the all pairwise comparison Dunn's test in *F* and *G*, unpaired *t* test (*black line* in *F*), paired *t* test or Wilcoxon Signed Rank Test in *H*).

at −100 mV) but significantly potentiated histamine-induced $TRPC5_{Y541A}$ currents (Fig. 6, *A*, *G*, and *H*).

We next assessed whether any of the other aromatic residues, such as Phe-540 and Tyr-542, regulate either the Gd^{3+} or $G_{q/11}$-PLC activation sensitivity of TRPC5. In HEK-$TRPC5_{Y542A}$ cells, we observed large slowly developing GTPγS-induced currents exhibiting a TRPC5-like current-voltage relationship (Fig. 5*D*). The GTPγS-activated inward TRPC5-like currents were also observed in HEK-$TRPC5_{F540A}$ cells, but they had significantly smaller current densities (Fig. 5, *E* and *F*). 100 μM Gd^{3+} significantly potentiated the GTPγS-activated currents through $TRPC5_{F540A}$ (2.7-fold increase at −100 mV and 1.3-fold change at +100 mV; Fig. 5, *E*, *G*, and *H*). Conversely, Gd^{3+} potently inhibited the $TRPC5_{Y542A}$ currents (0.3-fold change at −100 mV and 0.5-fold change at +100 mV, Fig. 5, *D*, *G*, and *H*), suggesting that the Y542A mutant completely lacks Gd^{3+} potentiation but is still a subject of the Gd^{3+}-dependent pore block. The $TRPC5_{Y541A}$, $TRPC5_{F540A}$, and $TRPC5_{E543Q}$ mutants' relative Ca^{2+} permeability (P_{Ca}/P_{Na} = 1.55 ± 0.15, 1.68 ± 0.10, and 1.45 ± 0.16, respectively) was not different from that of wild type TRPC5 (P_{Ca}/P_{Na} = 1.63 ± 0.16). Conversely, $TRPC5_{Y542A}$ exhibited a slightly higher relative Ca^{2+} permeability (P_{Ca}/P_{Na} = 2.77 ± 0.24).

We also investigated the effects of Gd^{3+} on histamine-induced currents in HEK cells expressing the $TRPC5_{F540A}$, $TRPC5_{Y542A}$, $TRPC5_{E543Q}$, and $TRPC5_{R545A}$ mutants (Fig. 6, *B–E*, *G*, and *H*). Histamine-induced currents in HEK cells expressing all of the tested mutants except $TRPC5_{F540A}$ exhibited densities similar to that observed in HEK-TRPC5 cells (Fig. 6*F*). However, HEK-$TRPC5_{F540A}$ cells exhibited significantly smaller histamine-induced currents. Gd^{3+} markedly potentiated histamine-induced currents in HEK-$TRPC5_{F540A}$ and HEK-$TRPC5_{R545A}$ cells (Fig. 6, *D*, *E*, *G*, and *H*), whereas Gd^{3+} inhibited histamine-induced currents in HEK-$TRPC5_{Y542A}$ and HEK-$TRPC5_{E543Q}$ cells (Fig. 6, *B*, *C*, *G*, and *H*). Thus, these data indicate that the Tyr-542 residue is critical for establishing the functional eCBS, whereas the Tyr-541 residue appears to only slightly modulate TRPC5's Gd^{3+} sensitivity. Alternatively,

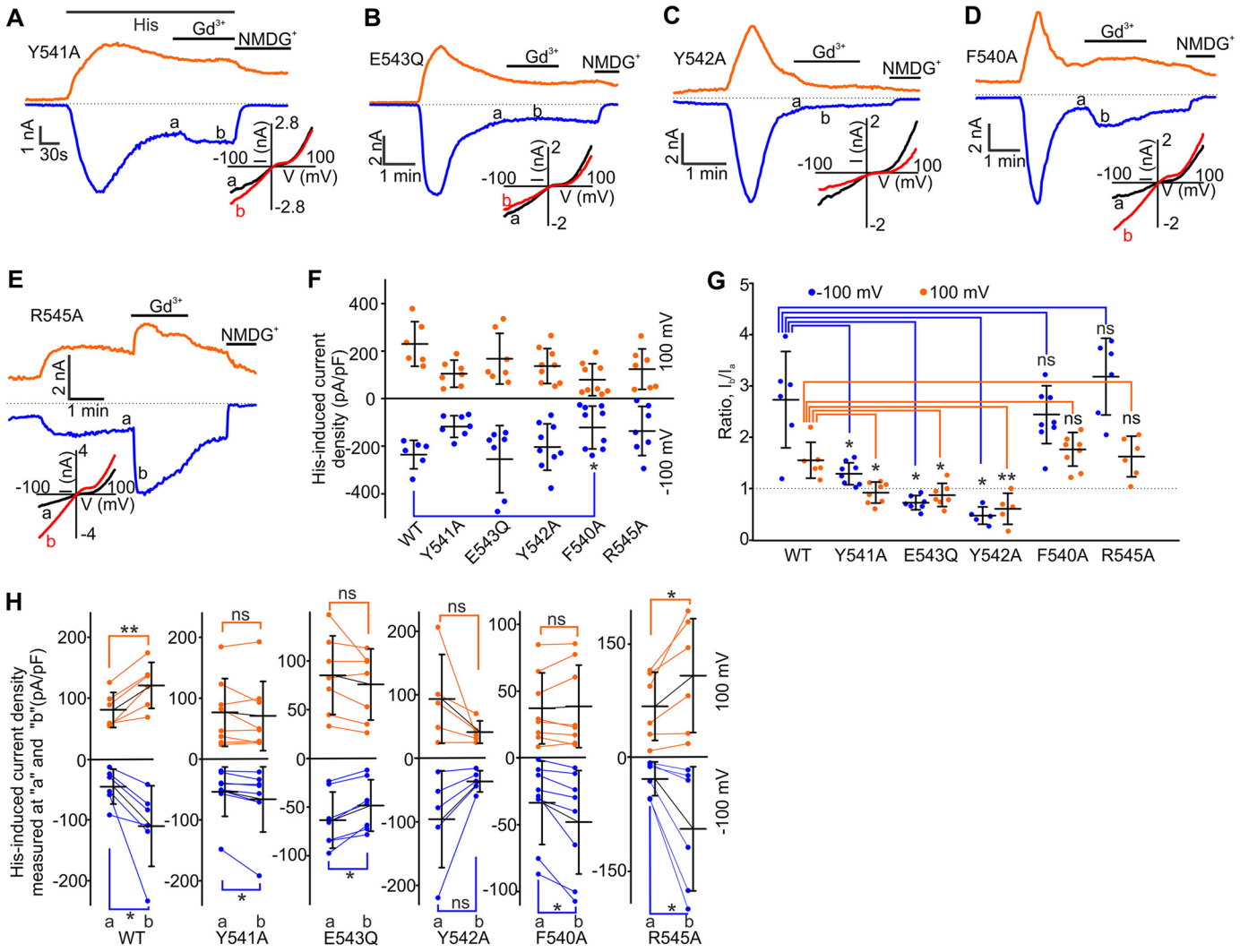

FIGURE 6. **Effects of Gd^{3+} on histamine-activated currents mediated by mouse TRPC5, $TRPC5_{Y541A}$, $TRPC5_{E543Q}$, $TRPC5_{Y542A}$, $TRPC5_{F540A}$, and $TRPC5_{R545A}$.** *A–E*, time courses of the whole-cell currents induced by 5 μM histamine in HEK cells overexpressing one of the mutants listed above. Gd^{3+} (100 μM) and NMDGCl were added at the times indicated by the *horizontal bars*. *Insets* show the current-voltage relations. *F*, comparison of the mean current densities of histamine-induced currents recorded at −100 mV (*blue dots*) and +100 mV (*orange dots*) in HEK cells transfected with TRPC5-WT, $TRPC5_{Y541A}$, $TRPC5_{Y542A}$, $TRPC5_{F540A}$, $TRPC5_{E543Q}$, or $TRPC5_{R545A}$. *G* and *H*, summary data of current ratios and current densities measured at the time points of *a* and *b* at holding potentials of −100 mV (*blue dots*) and +100 mV (*orange dots*) for the data sets shown in *A–E*. The ratios represent the relative current amplitude increases in the presence of Gd^{3+}. In all six plots of *H*, the *y* axis label is *Histamine-induced current density measured at a and b (pA/pF)*. The *error bars* represent standard deviation, and the mean values are indicated with *horizontal bars* (*, $p < 0.05$; **, $p < 0.01$, *ns* stands for not significant; one-way ANOVA on Rank followed by the all pairwise comparison Dunn's test in *F* and *G*, paired *t* test or Wilcoxon Signed Rank Test in *H*).

the Phe-540 and Arg-545 residues do not affect Gd^{3+} sensitivity of TRPC5.

A Mechanism Regulating Ca^{2+} Permeability in TRPC5—According to our model of the TRPC5 pore region (Fig. 4*C*), the Asn-584 residue occupies a position within the pore loop that is homologous to that of the Asp-646 residue in TRPV1 (19). It was demonstrated (27) that the TRPV1 pore loop's Asp-646 residue forms the channel's selectivity filter. Indeed, the TRPV1 cryo-EM structure (19) revealed that this exact residue faces the pore lumen and is likely to contribute to coordinating the hydrated cations passing through the pore of TRPV1. This suggested that Asn-584 may contribute to regulating Ca^{2+} permeability of TRPC5. Remarkably, in a sequence alignment of TRPV1 and TRPC5, the position homologous to Asp-646 is occupied by Asn-584, the same residue that faces the pore lumen of TRPC5 in our homology model (Figs. 4, *C* and 7*A*). This persuaded us to examine whether the Asn-584 residue plays any role in modulating TRPC5's Ca^{2+} permeability.

To assess the contribution of Asn-584 to regulating the Ca^{2+} selectivity of TRPC5, we mutated this residue to either aspartate or glycine. First, we used histamine to stimulate TRPC5 and its mutants' activity. In HEK-$TRPC5_{N584D}$ and HEK-$TRPC5_{N584G}$ cells, the histamine-induced current densities were comparable with those observed in HEK-TRPC5 cells ($I_{TRPC5} = -14.34 \pm 5.05$ pA/pF, $I_{N584D} = 14.13 \pm 3.1$ pA/pF, and $I_{N584G} = 15.75 \pm 4.9$ pA/pF at −100). Gd^{3+} markedly potentiated the histamine-induced $TRPC5_{N584D}$ and $TRPC5_{N584G}$ currents (the -fold changes are 3.73 ± 0.58 for TRPC5, 4.03 ± 0.68 for $TRPC5_{N584D}$, and 2.67 ± 0.35 for $TRPC5_{N584G}$ at −100 mV; Fig. 7, *B–D*). We next determined the reversal potentials of the histamine-induced

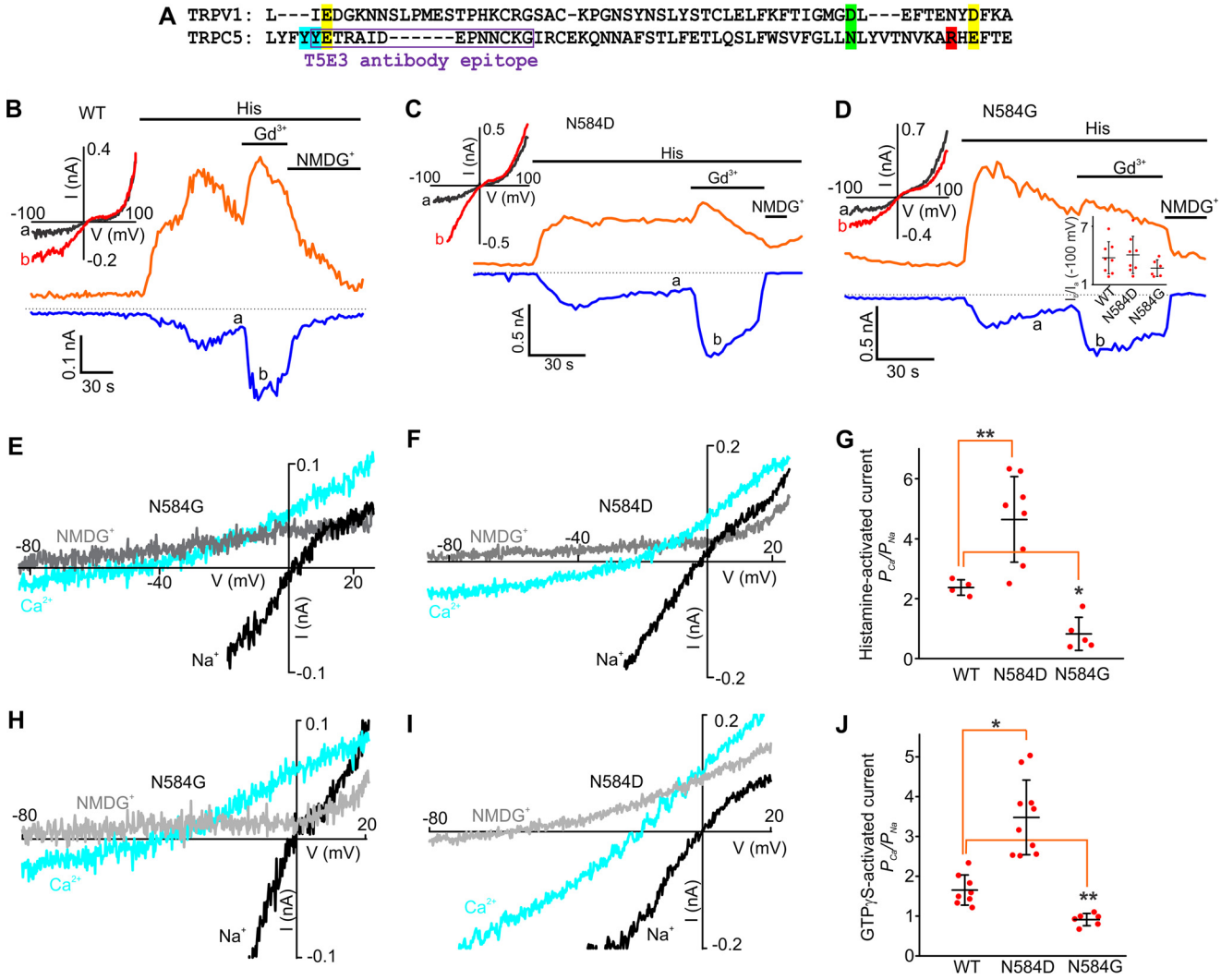

FIGURE 7. **The Asn-584 residue determines Ca^{2+} permeability in TRPC5.** *A*, amino acid sequence alignment of TRPC5 (Leu-538 through Glu-598) and TRPV1. The epitope of the T5E3 antibody is indicated in the sequence with a *purple box*. The Glu-543 and Glu-595 residues in TRPC5 are highlighted in *yellow*. The Arg-593 residue in TRPC5 is highlighted in *red*. The Asn-584 residue in TRPC5 and the Asp-646 residue in TRPV1 are highlighted in *green*. The Tyr-541 and Tyr-542 residues in TRPC5 are highlighted in *sky blue*. *B–D*, sample traces of time courses of the histamine-induced currents through human TRPC5, human $TRPC5_{N584D}$, and human $TRPC5_{N584G}$ mutants. Histamine (5 μM), Gd^{3+} (100 μM), and NMDGCl were added at the times indicated by the *horizontal bars*. The *broken black lines* indicate the level of the zero current. The *upper* and *lower traces* represent the outward and inward whole cell currents recorded at +100 mV (*orange lines*) and −100 mV (*blue lines*). The *inset* in *D* shows the summary data of current ratios measured at the time points of *a* and *b* at the holding potentials of −100 mV. *E*, *F*, *H*, and *I*, current-voltage relations of $TRPC5_{N584D}$ and $TRPC5_{N584G}$ currents acquired at the time points with 10 mM Ca^{2+} (*sky blue lines*) and with 150 mM NaCl (*black lines*) in the solution. The currents are activated by GTPγS (*E* and *F*) or histamine (*H* and *I*). *G* and *J*, summary data showing the Na^+ and Ca^{2+} permeability ratio for $TRPC5_{N584D}$ and $TRPC5_{N584G}$ currents activated by GTPγS and histamine as compared with that for TRPC5. The *vertical error bars* represent standard deviation, and the mean values are indicated with *horizontal bars* (*, $p < 0.05$; **, $p < 0.01$; one-way ANOVA followed by the all pairwise comparison Student-Newman-Keuls test).

currents in HEK-TRPC5, HEK-$TRPC5_{N584D}$, and HEK-$TRPC5_{N584G}$ cells bathed in 150 NaCl- or 10 $CaCl_2$-containing extracellular solutions to quantify Ca^{2+} permeability of TRPC5 and the pore mutants. We found that the relative Ca^{2+} permeability P_{Ca}/P_{Na} of $TRPC5_{N584D}$ was ~5.7-fold higher (4.65 ± 0.50; Fig. 7, *F* and *G*) than that of $TRPC5_{N584G}$ (0.82 ± 0.25; Fig. 7, *E* and *G*) and ~2-fold higher than that of the wild type human TRPC5 (2.37 ± 0.13; Fig. 7*G*). Next, we determined the values of the relative Ca^{2+} permeability P_{Ca}/P_{Na} of TRPC5 and its pore mutants when the currents were activated by GTPγS (Fig. 7, *H–J*). The relative Ca^{2+} permeability P_{Ca}/P_{Na} of TRPC5, $TRPC5_{N584D}$, and $TRPC5_{N584G}$ was 1.65 ± 0.13, 3.48 ± 0.30, and 0.91 ± 0.06, respectively. These data support the hypothesis that the asparagine 584 contributes to regulating the Ca^{2+} permeability of TRPC5 and provides further evidence of the predictive potential of the TRPC5 model described in this study.

Discussion

We provide evidence that the Arg-593 residue is critical for conferring GPCR-$G_{q/11}$-PLC-dependent activation sensitivity on TRPC5. We used computer modeling to generate a three-dimensional structure model of the TRPC5 channel that was used to guide our mutagenesis efforts. Validating the model, we additionally identified two aromatic tyrosine, Tyr-541 and Tyr-54293 residues, important for fine-tuning Gd^{3+} sensitivity or establishing the functional eCBS, and showed that the Asn-584 residue is critical for controlling Ca^{2+} permeability of TRPC5.

Our modeling data suggest that in the absence of a trivalent cation, Arg-593 may cross-bridge the E3 and E4 loops in TRPC5 by interacting with either the carboxyl group of Glu-543 and the main-chain carbonyl oxygen of the Thr-544 (Fig. 4, *B* and *D*) or both Glu-543 and Glu-595 residues at the same time (Fig. 4, *B* and *E*). Indeed, the guanidinium moiety of arginine is well known to participate in the formation of various bridges in proteins (21). The ability of Arg-593 to interact with the main-chain carbonyl oxygen of the Thr-544 may explain the findings (18) that the Glu-543 and the double E543Q/E595Q mutants of TRPC5 are still GPCR-$G_{q/11}$-PLC activation-sensitive.

The importance of the E3 and E4 loop cross-bridging for controlling $G_{q/11}$-PLC activation sensitivity of TRPC5 is supported by the fact that the E3 loop-targeted anti-TRPC5 (T5E3) antibody, developed in the Beech laboratory (29), inhibits TRPC5 activity by binding to an E3 loop epitope (*YETRAIDEPNNCKG*; Fig. 7*A*) that contains the Tyr-542 and Glu-543 residues (underlined). The binding of the T5E3 antibody to the epitope most likely obstructs the E3 and E4 loop cross-bridging. We propose that this disrupts the transmission of the gating effort force to the pore helix-loop unit, with the Arg-593 bridge playing a role of the "molecular fulcrum."

We speculate that Gd^{3+} likely emulates the guanidinium moiety of Arg-593 and competes with the group within the eCBS. When the trivalent cation displaces the guanidinium moiety of Arg-593 in the eCBS, the cation likely coordinates with Glu-543 and Glu-595 residues (Fig. 4, *E* and *F*), facilitating the long range conformational changes that are induced by GPCR-$G_{q/11}$-PLC-mediated activation of TRPC5. Consistently, we found that the Gd^{3+} effect on TRPC5 currents is markedly reduced at 42 °C (*a*; Fig. 8). This is likely due to a temperature-related increase in the Glu-543 and Glu-595 residues' kinetic energy leading to a reduced ability of Gd^{3+} for cross-bridging the E3 and E4 loops.

It was reported that histamine-induced TRPC5 currents were greater in the presence of extracellular Ca^{2+} as compared with those recorded under the Ca^{2+}-free condition (1), a phenomenon we also observed in wild type TRPC5 (Fig. 3, *A* and *B*). In HEK-$TRPC5_{R593A}$ cells, however, extracellular Ca^{2+} instead inhibited the small currents activated by histamine in the absence of Gd^{3+}. Jung *et al.* (16) demonstrated that very high extracellular Ca^{2+} concentrations (20 mM) potentiated TRPC5 currents by acting via the eCBS, suggesting that this site might serve as a sensor for extracellular Ca^{2+}. It is possible that the R593A mutation weakens the ability of the eCBS to bind extracellular Ca^{2+}, revealing the Ca^{2+} pore-blocking effect. Indeed, a homology model of the $TRPC5_{R593A}$ mutant (Fig. 9) suggests that in the mutant, the E3 and E4 loops may be separated by a distance of 11–13 Å between Glu-543 and Glu-595. Considering the distance for forming a salt bridge in proteins is <4 Å, it is possible that in contrast to Gd^{3+}, Ca^{2+} is incapable of cross-bridging the carboxyl moieties of Glu-543 and Glu-595 in $TRPC5_{R593A}$. Alternatively, the eCBS may not be sensitive to small changes of extracellular Ca^{2+} within the physiological range (<2 mM). Consistently, the $TRPC5_{E543Q}$ mutant was still potently activated by histamine and exhibited large currents as Jung *et al.* (16) also reported, despite the fact that the eCBS was destroyed. In this paper, Fig. 5*C* also shows the large GTPγS

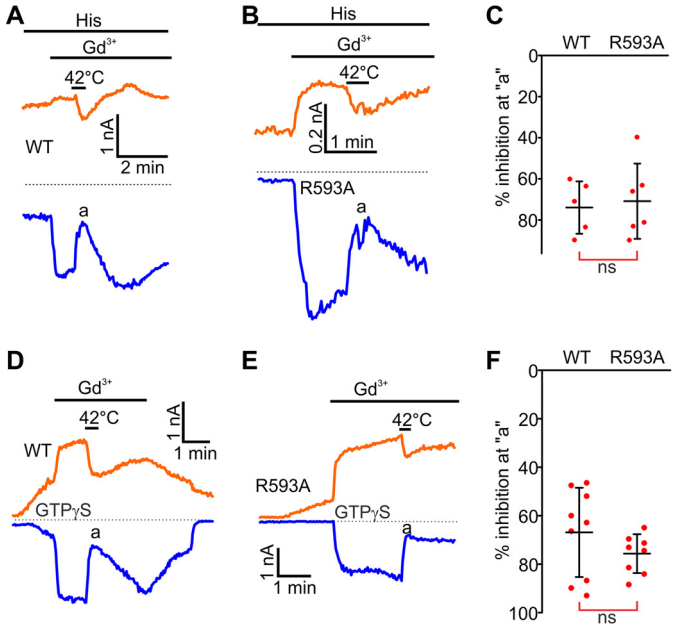

FIGURE 8. **Heating to 42 °C inhibits Gd^{3+}-potentiated mouse TRPC5 and mouse $TRPC5_{R593A}$ currents.** *A*, *B*, *D*, and *E*, sample traces of histamine and GTPγS-induced TRPC5 and $TRPC5_{R593A}$ currents. Gd^{3+} (100 μM) and the extracellular solution heated to 42 °C was added at the times indicated by the *horizontal bars*. The *broken black lines* indicate the level of the zero current. *C* and *F*, summary data for current inhibition by the extracellular solution heated to 42 °C ($V_{holding}$ = −100 mV, the *vertical error bars* represent standard deviation, and the mean values are indicated with *horizontal bars*; *ns* stands for not significant, Mann-Whitney Rank Sum Test).

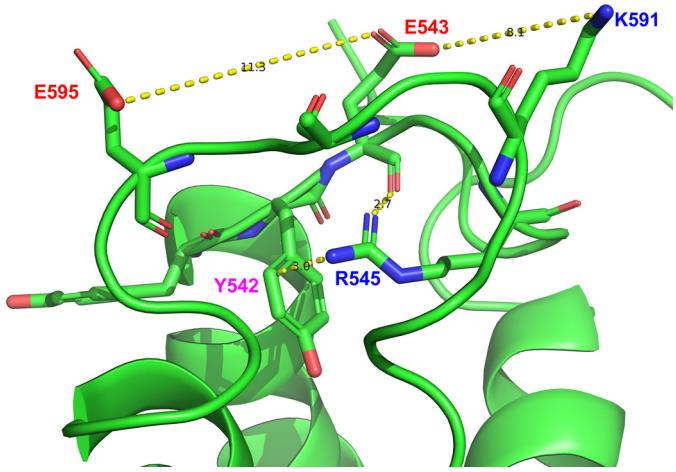

FIGURE 9. **A conformation of the open R593A mutant of mouse TRPC5.** The model predicts that in the mutant, the Glu-543 to Glu-595 cross-distance is ~11 Å. It is likely that Arg-545 may form a π-interaction with the Tyr-542 aromatic ring and a dipole-dipole interaction with the main-chain carbonyl moiety of Glu-543, whereas Lys-591 is too far (~8 Å) from Glu-543 to form a salt bridge.

infusion-induced $TRPC5_{E543Q}$ currents, indicating that the eCBS is unlikely the only extracellular Ca^{2+} sensor underlying the sensitivity of TRPC5 to extracellular Ca^{2+}. Indeed, the Clapham group presented evidence that there is an intracellular Ca^{2+} binding site on TRPC5 that is important for potentiating the channel activity by extracellular Ca^{2+} (30).

There is another positively charged residue, Lys-591, that is located near Arg-593 (Fig. 5*A*). However, it appears that the Lys-591 residue is less important for bridging the E3 and E4 loops. Indeed, in the model (Fig. 9), it rather interacts with the

adjacent TRPC5's subunit and is located too far from both Glu-543 and Glu-595. We cannot rule out that in some conformations Lys-591 may still interact with Glu-543 or carbonyls of the E3 loop main chain cross-bridging the E3 and E4 loops. However, we observed a markedly reduced sensitivity to $G_{q/11}$-PLC-dependent activation in the R593A mutant despite the fact that the mutant possesses the Lys-591 residue. Thus, Lys-591 may be responsible for some small residual $G_{q/11}$-PLC activation sensitivity of the R593A mutant of TRPC5 but cannot fully substitute the Arg-593 residue.

Flockerzi and co-workers (31) recently demonstrated that a substitution of the conserved glycine 504 located within TRPC5's intracellular S4-S5 linker to a serine resulted in a fully active mutant. This implicates the intracellular S4-S5 linker of TRPC5 as a part of the "cardan chain" of the gating machinery that opens the channel. In TRPC5, the S5 transmembrane domain communicates directly with the long E3 extracellular loop that continues into the pore helix and then the pore loop, which is in turn connected to the S6 transmembrane domain. The existence of the long flexible E3 extracellular loop in TRPC5 may dampen the signal transmission from S5 to the pore loop. The bridging of the E3 and E4 loops by the Arg-593 residue would make the structure more rigid. Thus, Arg-593 may be a regulator of the rigidity of the TRPC5 transmission system communicating the signals from either the S5 or S6 domain to the pore helix-loop unit. Stronger Gd^{3+}-dependent bridging of the E3 and E4 extracellular loops would likely result in a further increased rigidity of TRPC5 at the bridging site. Interestingly, a reduced single-channel flickering was associated with the increased rigidity of the pore loop (19). Remarkably, Gd^{3+} binding to the eCBS indeed increases the mean open time of TRPC5 single channel events (16).

Among TRPC channels, TRPC5 is the only channel that has the positively charged residue at the position 593. At the homologous positions, other TRPC channels possess either neutral (glycine in TRPC1, glutamine in TRPC4, or asparagine in TRPC6) or negatively charged (aspartic acid in TRPC7; Fig. 5*A*) residues. Conversely, most of TRPCs have a conserved lysine at the homologous position to that of TRPC5's Lys-591 (Fig. 5*A*). It is possible that Lys-591 can be important for cross-linking E3 and E4 loops in other TRPC channels.

Notably, it was reported (19) that the extracellular resiniferatoxin/double-knot toxin-induced activation of the TRPV1 channel requires the separation of the two TRPV1's glutamate residues Glu-600 and Glu-654 that are homologous to the TRPC5's Glu-543 and Glu-595. This is opposite to what we observe in TRPC5, where cross-bridging of Glu-543 and Glu-595 appears to potently increase TRPC5 channel activity, but it is consistent with the fact that neither resiniferatoxin nor double-knot toxin activates TRPC5. Thus, the different members of the TRP family may utilize diverse mechanisms regulating channel activation.

Our data indicate that the aromatic residues, Tyr-541 and Tyr-542, play critical roles in regulating or establishing the functional eCBS in TRPC5. The evidence that Tyr-542 is more important than Tyr-541 in controlling TRPC5's Gd^{3+} sensitivity is consistent with our TRPC5 model, suggesting that the main-chain carbonyl group of Tyr-542 may directly contribute to coordinating Gd^{3+} within the eCBS (Fig. 4, *E* and *F*). We propose that Tyr-541 and Tyr-542 may stabilize the E3 loop through hydrophobic effects and strategic positioning of the Glu-543 residue against the Glu-595 residue. This appears to be crucial for enabling proper Gd^{3+}-coordination within the eCBS. Remarkably, TRPC3, TRPC4, TRPC6, and TRPC7 channels also have a cluster of tyrosines at the homologous positions to those of TRPC5's Tyr-541 and Tyr-542. This suggests that these conserved tyrosines may also be important for regulating the function of other TRPC channels.

Gd^{3+} is not a usual constituent of the extra-neuronal fluids. However, its profound effect on TRPC5 activity leads us to believe that there might be a yet unidentified small molecule, which is co-released with a common neurotransmitter during increased firing activity, to act on the eCBS of TRPC5 and to modulate neuronal activity. We speculate that the eCBS of TRPC5 might play a physiological role in fine-tuning the synaptic strength or modulating some forms of synaptic plasticity involving the indirect metabotropic chemical synapses. Conversely, TRPC5 hyperactivation may contribute to toxicity associated with divalent cations such as Pb^{2+} (17). An increased cross-bridging of the eCBS residues by trivalent cations may lead to the generation of prolonged depolarization and bursting, resulting in imbalance in neuronal networks, culminating in the epileptiform seizure discharges. Remarkably, the accidental intrathecal administration of Gd^{3+}-containing contrast reagents (Omniscan and Magnevist) for enhancing magnetic resonance imaging was associated with seizures in human patients (32, 33).

While validating our homology model of TRPC5, we found that the Asn-584 residue is a part of the selectivity filter of TRPC5. This asparagine residue is homologous to the negatively charged aspartate 646 in TRPV1, which was identified as the molecular determinant of TRPV1's Ca^{2+} permeability (19). Although it is unusual that a non-charged residue determines Ca^{2+} permeability of a cation channel, asparagine does possess a polar amide moiety that has a partial negative charge on its oxygen atom, probably contributing to coordinating and partially dehydrating conducting cations in TRPC5's selectivity filter. The fact that there is no negatively charged residue in the selectivity filter of TRPC5 is consistent with the observation that TRPC5 has a 5-fold smaller relative permeability ratio of P_{Ca}/P_{Na} than TRPV1 (P_{Ca}/P_{Na} ~10 for TRPV1 and ~2 for TRPC5 (28)). Thus, asparagine residues may regulate Ca^{2+} permeability in weakly Ca^{2+}-permeable non-selective cation channels.

In sum, we propose that the arginine Arg-593 serves as the molecular fulcrum, allowing the efficient transmission of the GPCR-$G_{q/11}$-PLC-powered gating effort force to the pore helix-loop unit of TRPC5. These data provide the first molecular insight into the mechanisms regulating GPCR-$G_{q/11}$-PLC activation sensitivity of a receptor-operated channel.

Experimental Procedures

Molecular Biology—The mouse (accession #NM_009428) and human (accession #NM_012471, Origene Technologies, Rockville, MD) TRPC5 cDNAs were used during this study. All TRPC5 mutants were generated using the Lightening

QuikChange site-directed mutagenesis kit (Agilent Technologies, Santa Clara, CA) according to the manufacturer's recommendations. All mutations were verified by sequencing.

HEK Cell Culture and Transfection—HEK cells (American Type Culture Collection, Manassas, VA) were cultured in Eagle's minimum essential medium supplemented with 10% fetal bovine serum. HEK cells were transfected using the Lipofectamine 3000 reagent (Invitrogen) in accordance with the manufacturer's instruction. The transfection mixture contained 4 μg of each channel cDNA and 0.25 μg of the histamine H1 receptor. The transfected cells were cultured for 24–48 h before electrophysiological experiments.

Homology Modeling and Molecular Dynamics—The homology modeling and molecular dynamics simulations were performed using the Accelrys Discovery Studio software package (Accelrys, Inc., San Diego, CA). The cryoEM-derived structures of the rat TRPV1 protein in and the open state (PDB ID: 3J5Q) were used as the templates to build homology models of the truncated tetrameric TRPC5 channel that contained the four S5-P-loop-S6 regions except the residues between asparagines 552 and 562 in the E3 extracellular loop. TRPC5 and TRPV1 exhibit 26.8% identity within their S5-P-loop-S6 segments. After the homology model was constructed, the plasma membrane was added, and the CHARMm forcefield was applied to the molecule using the Momany-Rone method to assign the partial charges. Then the standard dynamics cascade was performed that included the following steps: 1) minimization with steepest descent, 2) minimization with conjugate gradient, 3) dynamics with heating, 4) equilibration dynamics, and 5) production dynamics. In some cases Gd^{3+} was added to the molecule before performing molecular dynamics simulations. The default parameters of Discovery Studio were used. During the molecular dynamic simulations, 1-ns trajectories were carried out and analyzed.

Patch Clamp Electrophysiology—An Axopatch 200B amplifier and Digidata 1550A digitizer (Molecular Devices) were used to record TRPC5 currents in the whole-cell patch clamp mode. The sampling rate was 1 kHz, and the currents were filtered at 3 kHz. Series resistance compensation was set to 50–70%. The pCLAMP 10 software package was used for acquisition control and data analyses. An episodic stimulation voltage protocol was employed. Cells were voltage-clamped at a holding potential of −60 mV, and the voltage ramps from −100 to +100 mV were applied with 2-s intervals. In the indicated experiments each voltage ramp from −100 to +100 mV was followed by a brief 50-ms depolarizing pulse to +150 mV. TRPC5 currents were activated either by a bath application of 40 μM histamine or by a dialysis with 500 μM GTPγS added directly into the pipette solution. Current traces from cells where the leak current exceeded 100 pA and/or the access resistance was >10 megaohms were not analyzed. To quantify Gd^{3+} effects on TRPC5 activity, we calculated the ratio of the current values acquired before and in the presence of the trivalent cations. Relative permeability values (P_{Ca}/P_{Na}) were calculated using the equation,

$$P_{Ca}/P_{Na} = ([Na^+]_0/4[Ca^{2+}]_0) \times \exp((F \times (E_{Ca^{2+}} - E_{Na^+})/RT) \times (1 + \exp((F \times E_{Ca^{2+}})/RT) \quad \text{(Eq. 1)}$$

where E_{Na+} and E_{Ca2+} are the reversal potentials of TRPC5 currents acquired in extracellular solutions of 150 NaCl and 10 Ca-NMDG, respectively. R, T, and F have their established meanings. The current densities were calculated by dividing the current amplitude values by the cell capacitance. All of the electrophysiological experiments were performed at room temperature (22–25 °C).

Solutions—The standard external solution contained 145 mM NaCl, 2.5 mM KCl, 2.0 mM $CaCl_2$, 1 mM $MgCl_2$, 10 mM HEPES, and 5.5 mM glucose (pH 7.2 adjusted with NaOH). The standard pipette solution contained 125 mM $CsMeSO_3$, 3.77 mM $CaCl_2$, 2 mM $MgCl_2$, 10 mM EGTA (100 nM free Ca^{2+}), and 10 mM HEPES (pH 7.2 adjusted with Trizma base (Tris base)). The $NMDG^+$ solution contained 150 mM NMDG-Cl, 10 mM HEPES, and 5.5 mM glucose (pH 7.2 adjusted with Trizma base). The 150 NaCl solution contained 150 mM NaCl, 10 mM HEPES, 0.5 mM EGTA, and 5.5 mM glucose (pH 7.2 adjusted with Trizma base). The 10 $CaCl_2$ solution contained 135 mM NMDG-Cl, 10 mM $CaCl_2$, 10 mM HEPES, and 5.5 mM glucose (pH 7.2 adjusted with Trizma base). The osmolarity of all solutions was adjusted to 300–305 mosM with mannitol if it was needed.

Cell-surface Protein Biotinylation and Western Blotting—Transfected HEK cells were culture in 35-mm tissue culture dishes for 48 h in a CO_2 incubator as described above. Before biotinylation, the culture medium was aspirated and the cells were washed three times with 1 ml of ice-cold PBS. After washing, 0.5 ml of 50 μM biotin-X-NHS (biotin N-hydroxysuccinimide-sulfo ester containing a 6-aminocaproic acid "X" spacer arm; EMD Millipore, Billerica, MA) in PBS was added to the cells. A Petri dish with cells bathed in the biotinylating solution was then placed on an orbital shaker to gently agitate for 30 min at 4 °C. Cells were then washed 3 times with 1 ml of ice-cold PBS supplemented with 100 mM glycine (quenching solution) and gently agitated for 5 min at room temperature followed by additional washes with 1 ml of PBS. Cells were lysed on ice in 200 μl of the Thermo Fisher radioimmune precipitation assay buffer supplemented with the halt proteinase inhibitor mixture (Thermo Fisher Scientific, Waltham, MA), phenylmethylsulfonyl fluoride (Thermo Fisher Scientific), and 2% Triton X-100, avoiding bubble formation. Protease inhibitors were used as described in the manufacturer's instructions. The lysate was spun down at 24,000 × *g* at 4 °C. 100 μl of pre-absorbed avidin-agarose bead suspension supplemented with 2% bovine serum albumin was added to the supernatant and rotated for 30 min at 4 °C, spun down, and washed 3 times with the complete lysis buffer (200 μl). 50 μl of SDS gel loading buffer supplemented with 1 mM DTT was added to the pelleted beads and heated at 70 °C for 5 min to free biotinylated proteins. Membrane lysates were separated by 10% SDS-polyacrylamide gel electrophoresis, and the resolved proteins were transferred onto polyvinylidene difluoride membrane (PVDF) (Immun-Blot, Bio-Rad). Membranes were blocked with StartingBlock blocking buffer (Thermo Fisher Scientific) for 1 h at room temperature and then incubated overnight at 4 °C with either the primary polyclonal rabbit TRPC5 antibody diluted 1:2,000 in StartingBlock buffer (Alomone Labs, ACC-020) or the primary polyclonal rabbit Na^+,K^+-ATPase antibody (#3010, 1:750, Cell Signaling

Technology). Then PVDF membranes were washed 3 times and further incubated with an anti-rabbit secondary antibodies conjugated with the horseradish peroxidase (Cell Signaling, Danvers, MA; #7074; diluted 1:10,000) for 1 h at room temperature. The PVDF membranes were developed by using a Super-Signal West Pico enhanced chemiluminescence Kit (Pierce) according to the manufacturer's instructions.

Drugs—Histamine, $GdCl_3$, and other salts used in the experimental solutions were purchased from Sigma.

Statistical Methods—Sigma Plot 13 (Systat software, Inc.) was used for the statistical analyses. The unpaired *t* test was utilized to determine whether there is a statistically significant difference between the two data sets with normally distributed populations and equal variances. The Mann-Whitney Rank Sum Test was used to determine whether there is a statistically significant difference between the two data sets consisting of non-normally distributed populations with different variances. The paired *t* test was used to determine whether there is a statistically significant difference between the data sets before and after application, provided there were normally distributed populations with equal variances. The Wilcoxon Signed Rank Test was used to determine whether there is a statistically significant difference between the data sets before and after application, provided there were non-normally distributed populations with different variances. The one-way ANOVA test followed by a post hoc all pairwise multiple comparison test was used to determine whether there is a statistically significant difference between multiple groups presenting normally distributed populations with equal variances, whereas the one-way ANOVA on Rank test followed by a post hoc all pairwise multiple comparison test was used to determine whether there is a statistically significant difference between multiple groups presenting non-normally distributed populations with different variances. The data sets were considered significantly different if the *p* value was <0.05. In the text the data are presented as the means ± S.E. unless stated otherwise.

Author Contributions—A. G. O. conceived this work. X. C. and A. G. O. designed the experiments. X. C., W. L., and S. C. performed the experiments. X. C. analyzed the data. A. M. R. performed site-directed mutagenesis. M. S. and A. G. O. performed homology modeling. A. G. O. performed molecular dynamics simulations. C. W. S. carried out cell-surface biotinylation experiments and performed Western blots. X. C. and A. G. O. wrote the paper.

Acknowledgments—We thank Drs. Michael Schaefer and Jean-Charles Schwartz for mouse TRPC5 and the mouse histamine H1 receptor cDNAs, respectively. We thank Dr. Theodore R. Cummins for critical reading of the manuscript and valuable suggestions.

References

1. Okada, T., Shimizu, S., Wakamori, M., Maeda, A., Kurosaki, T., Takada, N., Imoto, K., and Mori, Y. (1998) Molecular cloning and functional characterization of a novel receptor-activated TRP Ca^{2+} channel from mouse brain. *J. Biol. Chem.* **273,** 10279–10287
2. Sossey-Alaoui, K., Lyon, J. A., Jones, L., Abidi, F. E., Hartung, A. J., Hane, B., Schwartz, C. E., Stevenson, R. E., and Srivastava, A. K. (1999) Molecular cloning and characterization of TRPC5 (HTRP5), the human homologue of a mouse brain receptor-activated capacitative Ca^{2+} entry channel. *Genomics* **60,** 330–340
3. Greka, A., Navarro, B., Oancea, E., Duggan, A., and Clapham, D. E. (2003) TRPC5 is a regulator of hippocampal neurite length and growth cone morphology. *Nat. Neurosci.* **6,** 837–845
4. Bezzerides, V. J., Ramsey, I. S., Kotecha, S., Greka, A., and Clapham, D. E. (2004) Rapid vesicular translocation and insertion of TRP channels. *Nat. Cell Biol.* **6,** 709–720
5. Kumar, S., Chakraborty, S., Barbosa, C., Brustovetsky, T., Brustovetsky, N., and Obukhov, A. G. (2012) Mechanisms controlling neurite outgrowth in a pheochromocytoma cell line: The role of TRPC channels. *J. Cell. Physiol.* **227,** 1408–1419
6. Puram, S. V., Riccio, A., Koirala, S., Ikeuchi, Y., Kim, A. H., Corfas, G., and Bonni, A. (2011) A TRPC5-regulated calcium signaling pathway controls dendrite patterning in the mammalian brain. *Genes Dev.* **25,** 2659–2673
7. Riccio, A., Li, Y., Moon, J., Kim, K. S., Smith, K. S., Rudolph, U., Gapon, S., Yao, G. L., Tsvetkov, E., Rodig, S. J., Van't Veer, A., Meloni, E. G., Carlezon, W. A., Jr., Bolshakov, V. Y., and Clapham, D. E. (2009) Essential role for TRPC5 in amygdala function and fear-related behavior. *Cell* **137,** 761–772
8. Zheng, F., and Phelan, K. D. (2014) The role of canonical transient receptor potential channels in seizure and excitotoxicity. *Cells* **3,** 288–303
9. Phelan, K. D., Shwe, U. T., Abramowitz, J., Birnbaumer, L., and Zheng, F. (2014) Critical role of canonical transient receptor potential channel 7 in initiation of seizures. *Proc. Natl. Acad. Sci. U.S.A.* **111,** 11533–11538
10. Tai, C., Hines, D. J., Choi, H. B., and MacVicar, B. A. (2011) Plasma membrane insertion of TRPC5 channels contributes to the cholinergic plateau potential in hippocampal CA1 pyramidal neurons. *Hippocampus* **21,** 958–967
11. Plant, T. D., and Schaefer, M. (2005) Receptor-operated cation channels formed by TRPC4 and TRPC5. *Naunyn Schmiedebergs Arch. Pharmacol.* **371,** 266–276
12. Schaefer, M., Plant, T. D., Obukhov, A. G., Hofmann, T., Gudermann, T., and Schultz, G. (2000) Receptor-mediated regulation of the nonselective cation channels TRPC4 and TRPC5. *J. Biol. Chem.* **275,** 17517–17526
13. Trebak, M., Lemonnier, L., DeHaven, W. I., Wedel, B. J., Bird, G. S., and Putney, J. W., Jr. (2009) Complex functions of phosphatidylinositol 4,5-bisphosphate in regulation of TRPC5 cation channels. *Pflugers Arch.* **457,** 757–769
14. Thakur, D. P., Tian, J. B., Jeon, J., Xiong, J., Huang, Y., Flockerzi, V., and Zhu, M. X. (2016) Critical roles of $G_{i/o}$ proteins and phospholipase Cδ1 in the activation of receptor-operated TRPC4 channels. *Proc. Natl. Acad. Sci. U.S.A.* **113,** 1092–1097
15. Venkatachalam, K., Zheng, F., and Gill, D. L. (2003) Regulation of canonical transient receptor potential (TRPC) channel function by diacylglycerol and protein kinase C. *J. Biol. Chem.* **278,** 29031–29040
16. Jung, S., Mühle, A., Schaefer, M., Strotmann, R., Schultz, G., and Plant, T. D. (2003) Lanthanides potentiate TRPC5 currents by an action at extracellular sites close to the pore mouth. *J. Biol. Chem.* **278,** 3562–3571
17. Sukumar, P., and Beech, D. J. (2010) Stimulation of TRPC5 cationic channels by low micromolar concentrations of lead ions (Pb^{2+}). *Biochem. Biophys. Res. Commun.* **393,** 50–54
18. Semtner, M., Schaefer, M., Pinkenburg, O., and Plant, T. D. (2007) Potentiation of TRPC5 by protons. *J. Biol. Chem.* **282,** 33868–33878
19. Cao, E., Liao, M., Cheng, Y., and Julius, D. (2013) TRPV1 structures in distinct conformations reveal activation mechanisms. *Nature* **504,** 113–118
20. Borders, C. L., Jr, Broadwater, J. A., Bekeny, P. A., Salmon, J. E., Lee, A. S., Eldridge, A. M., and Pett, V. B. (1994) A structural role for arginine in proteins: multiple hydrogen bonds to backbone carbonyl oxygens. *Protein Sci.* **3,** 541–548
21. Blondeau, P., Segura, M., Pérez-Fernández, R., and de Mendoza, J. (2007) Molecular recognition of oxoanions based on guanidinium receptors. *Chem. Soc. Rev.* **36,** 198–210
22. Blank, J. L., Ross, A. H., and Exton, J. H. (1991) Purification and characterization of two G-proteins that activate the beta 1 isozyme of phosphoinositide-specific phospholipase C. Identification as members of the G_q class. *J. Biol. Chem.* **266,** 18206–18216

23. Obukhov, A. G., and Nowycky, M. C. (2008) TRPC5 channels undergo changes in gating properties during the activation-deactivation cycle. *J. Cell. Physiol.* **216,** 162–171
24. Chen, X., Egly, C., Riley, A. M., Li, W., Tewson, P., Hughes, T. E., Quinn, A. M., and Obukhov, A. G. (2014) PKC-dependent phosphorylation of the H1 histamine receptor modulates TRPC6 activity. *Cells* **3,** 247–257
25. Obukhov, A. G., and Nowycky, M. C. (2004) TRPC5 activation kinetics are modulated by the scaffolding protein ezrin/radixin/moesin-binding phosphoprotein-50 (EBP50). *J. Cell Physiol.* **201,** 227–235
26. Obukhov, A. G., and Nowycky, M. C. (2005) A cytosolic residue mediates Mg^{2+} block and regulates inward current amplitude of a transient receptor potential channel. *J. Neurosci.* **25,** 1234–1239
27. García-Martínez, C., Morenilla-Palao, C., Planells-Cases, R., Merino, J. M., and Ferrer-Montiel, A. (2000) Identification of an aspartic residue in the P-loop of the vanilloid receptor that modulates pore properties. *J. Biol. Chem.* **275,** 32552–32558
28. Owsianik, G., Talavera, K., Voets, T., and Nilius, B. (2006) Permeation and selectivity of TRP channels. *Annu. Rev. Physiol.* **68,** 685–717
29. Xu, S. Z., Zeng, F., Lei, M., Li, J., Gao, B., Xiong, C., Sivaprasadarao, A., and Beech, D. J. (2005) Generation of functional ion-channel tools by E3 targeting. *Nat. Biotechnol.* **23,** 1289–1293
30. Blair, N. T., Kaczmarek, J. S., and Clapham, D. E. (2009) Intracellular calcium strongly potentiates agonist-activated TRPC5 channels. *J. Gen. Physiol.* **133,** 525–546
31. Beck, A., Speicher, T., Stoerger, C., Sell, T., Dettmer, V., Jusoh, S. A., Abdulmughni, A., Cavalié, A., Philipp, S. E., Zhu, M. X., Helms, V., Wissenbach, U., and Flockerzi, V. (2013) Conserved gating elements in TRPC4 and TRPC5 channels. *J. Biol. Chem.* **288,** 19471–19483
32. Kapoor, R., Liu, J., Devasenapathy, A., and Gordin, V. (2010) Gadolinium encephalopathy after intrathecal gadolinium injection. *Pain Physician* **13,** E321–E326
33. Park, K. W., Im, S. B., Kim, B. T., Hwang, S. C., Park, J. S., and Shin, W. H. (2010) Neurotoxic manifestations of an overdose intrathecal injection of gadopentetate dimeglumine. *J. Korean Med. Sci.* **25,** 505–508